Periodic networked imaging with nanoscale sensor nodes via two-layered time-division access

Shoma Nishibori, Tutomu Murase, *Member, IEEE,* and Yukihiro Tadokoro, *Senior Member, IEEE* .

***Abstract*—As the Internet of Things (IoT) has become a widespread phenomenon, promising sensor applications at the nanoscale have begun to emerge. One example is imaging via distributed massive nanoscale nodes (NSNs), which can be used to implement "invisible surveillance cameras" by, for example, painting liquids containing nanoscale sensors onto walls. This imaging method requires periodic data transfer from thousands of NSNs to a data collection node (DCN). An essential technique for handling such transfers is the media access control (MAC) protocol. However, existing protocols cannot support periodic transfer from numerous NSNs because of inefficient communication caused by a large amount of headers in the packets. In this paper, we introduce an original MAC protocol and discuss its capability in terms of implementing imaging applications. The proposed protocol applies a time-division access feature to reduce the amount of headers and a two-layered protocol to enable simultaneous transmission among nodes. Slot assignment is an essential function in time-division access and requires communication among nodes. Unlike existing methods, our simple approach enables communication by exploiting the unique features of the focused application. The results of the numerical simulation reveal that the proposed MAC protocol allows for periodic imaging with more than three thousand nodes and produces high-quality images very close to those obtained using ideal communication. These results are achieved by employing an original design framework to determine appropriate key parameters, such as number of clusters and frame rate.**

***Index Terms*—Internet of Nano Things, nanoscale sensor nodes, imaging, time-division access, clustering**

I. Introduction

THE age of the "Internet of Things (IoT)" is becoming a reality. The use of sensor devices to collect and communicate meaningful data, such as images and sounds enables a wide variety of valuable applications that can provide comfort and convenience [1]–[6]. Recent developments in nanotechnology have contributed to the miniaturization of sensor devices performing functions such as sensing and communication [7]–[19]. The remarkable progress to date offers the prospect of ultra-small wireless sensor nodes [12]–[17], suggesting the next phase of the IoT, namely, the Internet of Nano Things (IoNT) [20]–[28], which is expected to arrive in the next few decades. Under this framework, future applications that exploit nanoscale devices, including in-body monitoring of biological activity and environmental monitoring, are expected to be developed [28]–[30]. In particular, a promising application is the use of spatially distributed single-pixel cameras to provide "invisible imaging," that is imaging via a massive number of invisible nanoscale nodes (NSNs) [31]. Using compressed sensing techniques, periodically transmitted single-pixel data can be reconstructed into high-resolution images at a data collection node (DCN). Invisible imaging technology can lead to invisible monitoring and video recording applications that can be applied to autonomous driving, home security, and urban surveillance imaging.

It has been suggested that transferring the single-pixel data from thousands of NSNs is necessary to implement invisible imaging applications, primarily to obtain high-resolution images [31]. Such data would be transferred via wireless links, which would require periodic transfer using packets, to support video recording. An essential technique for handling this is the media access control (MAC) protocol. Unfortunately, to date, there exists no original work [31] that addresses an appropriate protocol for massive periodic transmissions. In the invisible imaging application, a transfer failure results in a lack of data required for reconstruction and a corresponding reduction in the quality of the obtained images. Accordingly, the protocol design should consider both the communication capability and the quality of the obtained images.

Enabling massive periodic transmission is challenging, as a multitude of transmissions within a specific time interval often leads to transmission errors, particularly packet collisions. The existing MAC protocols, including CSMA/CA and/or time-division access (TDA)-based protocols in wireless sensor and ad hoc networks, do not support such a massive periodic transmission (see Sec. VI). In CSMA/CA-based methods, redundant time intervals and long headers significantly decrease the data transfer capacity. Further, in TDA-based methods, efficient transfer is possible if the assignment of time slots is correctly established. However, this assignment requires a handshaking process among the nodes with CSMA/CA-based access [22], [32]–[39]; in a large-scale network containing a massive number of nodes, this process is difficult to implement.

A. Contribution of the present work

In this paper, a hierarchical MAC protocol, which we call two-layered time-division access (TL-TDA), is introduced, and the image quality that can be obtained using this approach is discussed. Our proposed method enables periodic data to be

S. Nishibori, T. Murase and Y. Tadokoro are with Graduate School of Informatics, Nagoya University, Nagoya, Aichi, 464-8603, Japan (e-mail: {nishibori@net., tom@}itc.nagoya-u.ac.jp).

Y. Tadokoro is also with the Toyota Central Research and Development Laboratories, Inc., Aichi 480-1192, Japan (e-mail: y.tadokoro@ieee.org).

Manuscript received April 30, 2020; revised June 18, 2021.

This paper has supplementary downloadable material provided by the authors available at http://ieeexplore.ieee.org. This material includes four multimedia AVI format movie clips showing the results of the video recording by the periodic imaging application. The total video size is 40 MB.

Copyright (c) 20xx IEEE. Personal use of this material is permitted. However, permission to use this material for any other purposes must be obtained from the IEEE by sending a request to pubs-permissions@ieee.org.

Digital Object Identifier xxxx/xxxxx

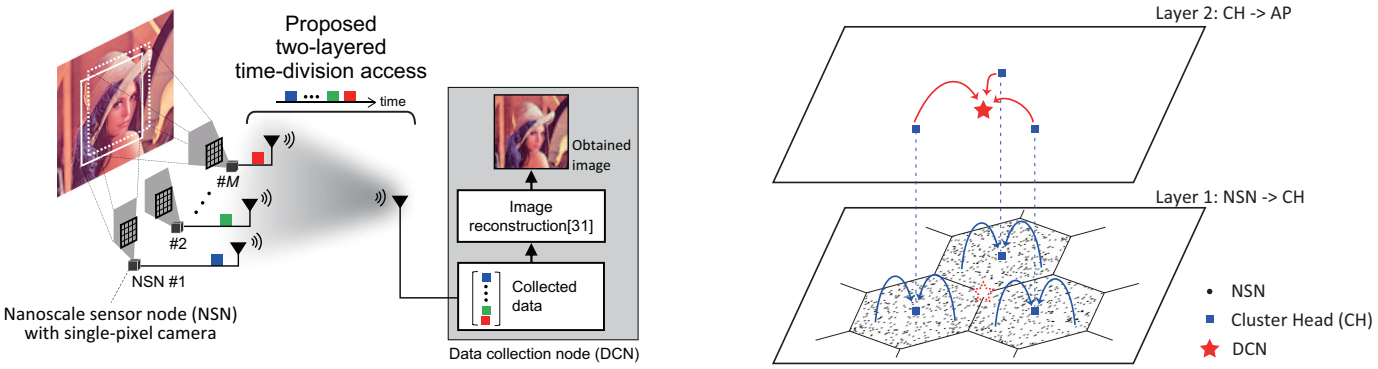

Fig. 1. (a) Networked imaging system with spatially distributed nanoscale sensor nodes (NSNs) accessed using proposed time-division approach. Each NSN is equipped with a single-pixel camera. Obtained pixel data are periodically transmitted to a data collection node (DCN)using the proposed two-layered time-division access (TL-TDA) protocol. At the DCN, the collected data are used to reconstruct images using an optimization method [31]. (b) Schematic of proposed TL-TDA protocol. Single-pixel data are transmitted from each NSN to a cluster head (CH) in Layer 1. In Layer 2, each CH aggregates the received data into a packet that is transmitted to the DCN. TDA is applied in both layers, with transmission timing provided by a DCN control station. This access method enables a significant reduction in header size because, under its centralized approach, it eliminates the long headers and redundant time intervals such as contention windows needed to avoid packet collision. The two-layered access also enables simultaneous transmissions from multiple NSNs, which improves Layer 1 capacity.

transferred from thousands of nodes using 1) a two-layered protocol with clustering, 2) a centralized approach with a control station, and 3) a simple handshaking method based on the unique node ID. Because a two-layered protocol with clustering enables simultaneous transmission between clusters, the proposed two-layered protocol achieves significant enhancements in the capacity. Further, owing to the centralized approach, the use of TDA enhances the performance by reducing the number of redundant time intervals and the header size. In addition, to assign time slots, a simple handshaking method is introduced. Unlike existing methods [36]–[38], our method does not require CSMA/CA-based access; instead, all communications for both negotiation and data transfer are established via TDA.

The key parameter in the proposed method is the number of clusters. We theoretically provide a design framework to determine the parameter that maximizes the data-collection rate, which is related to the frame rate of the captured video. The results of the numerical simulation reveal that the proposed TL-TDA protocol achieves a high reception rate even with more than three thousand nodes. This performance in data transfer enables the high quality of periodic imaging applications.

B. Notations and organization of the present paper

Notations employed throughout the present paper are listed in Tab. I.

The rest of this paper is organized as follows. In the next section, a brief overview of the focused imaging application is provided. In Sec. III, we describe the proposed MAC protocol in detail. A design method for determining the number of clusters—a key parameter—is theoretically derived in Sec. IV. Section V-A describes the scenario and parameter setup used to evaluate the proposed protocol, and the imaging performance is presented in Secs. V-B and V-C. A comprehensive review of the existing methods is provided in Sec. VI. Finally, we conclude the paper in Sec. VII.

TABLE I
NOTATIONS EMPLOYED THROUGHOUT THE PRESENT PAPER

Parameter	Description
B_{L1}	Bandwidth in Layer 1
B_{L2}	Bandwidth in Layer 2
H	The number of the cluster
H_{opt}	The optimal number of the cluster
L	The size of the data packet from NSNs
M	The total number of NSNs
M_i	The number of NSNs belonging to the i-th cluster
N_{L1}	The number of the time slots in Layer 1
N_{L2}	The number of the time slots in Layer 2
R_{I}	Imaging period
R_{L1}	Achievable data collection rate in Layer 1
R_{L2}	Achievable data collection rate in Layer 2
$R_{\mathrm{I_{opt}}}$	Optimum frame rate, (1)
T_{s}	Required time interval prior to transmission in the physical layer

II. OVERVIEW OF NETWORKED IMAGING SYSTEM WITH MASSIVE SPATIALLY-DISTRIBUTED NSNS

In this section, we provide a brief overview of the invisible imaging application described in this paper. Fig. 1(a) illustrates the networked imaging system with spatially distributed NSNs used to establish the application [31]. Each NSN is equipped with a single-pixel camera that can capture monochromatic images and subsequently convert them into three-byte single-pixel data. Following the proposed TL-TDA protocol, the obtained pixel data are periodically transmitted to a DCN wherein the collected data are used to reconstruct an image using an L1 optimization method. One advantage of this system is that, owing to their small size, the cameras can be easily installed at multiple locations. An example of this application

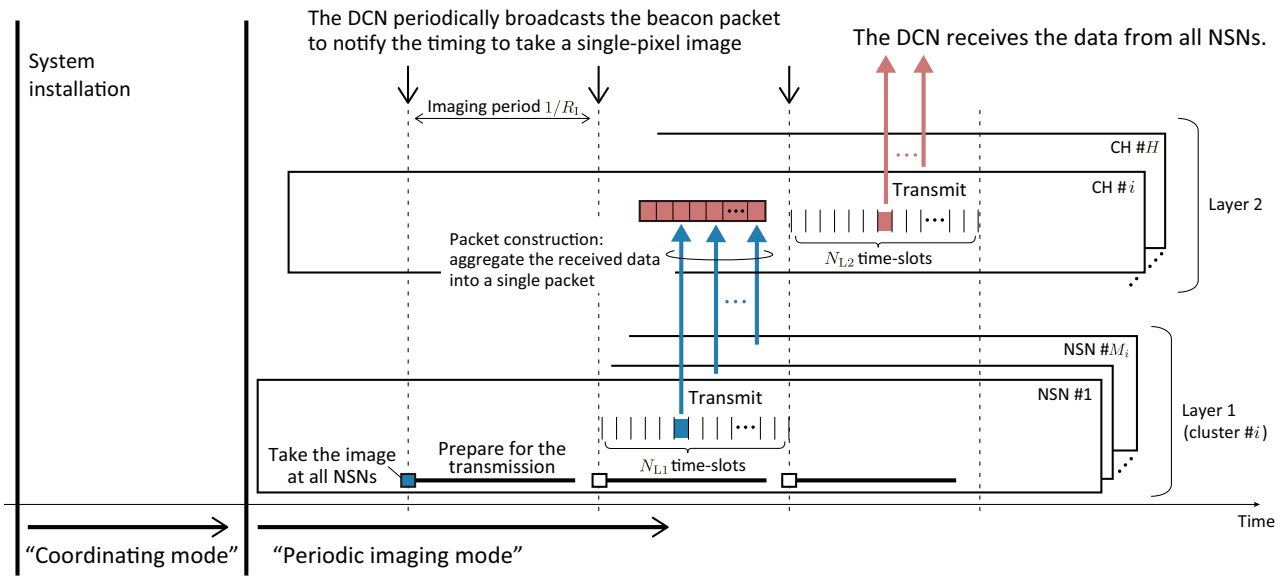

Fig. 2. Timing chart of proposed TL-TDA protocol. Following slot assignment during the coordinating mode, the NSNs periodically record single-pixel data following reception of a beacon packet from the DCN. Each NSN then sends these data to their assigned CH in the lower layer of Layer 1. The CH aggregates the received data into a single packet and then, in the upper layer of Layer 2, sends the packet to the DCN. In this process, the DCN collects data from all of the NSNs. TDA is employed in both layers, with N_{L1} and N_{L2} time-slots used in Layers 1 and 2, respectively. For simplicity, each layer is assumed to use different MHz-band frequencies for communication. It should be emphasized that the values of N_{L1} and N_{L2} strongly depend on the number of clusters and the frame rate.

is the installation of "invisible surveillance cameras" on a wall, which is achieved by painting a liquid containing invisibly small NSNs onto a surface. Another example is the use of "on-body" cameras to monitor obstacles surrounding a vehicle, wherein miniaturized cameras can even be painted onto a vehicle body.

The performance of the proposed application can be discussed in terms of both the quality of the reconstructed images and the frame rate. As described in [31], image quality deteriorates to a certain extent during the reconstruction step. This effect is often measured in terms of the peak signal-to-noise ratio (PSNR), which indicates the amount of noise present in a reconstructed image relative to its original image. For the DCN to reconstruct clear images with high PSNRs, a large number of NSNs should be able to successfully transmit their single-pixel data to the DCN. In such cases, transmission failure will result in a lack of information necessary for reconstruction. To evaluate the communication between the NSNs and the DCN, we employed the reception rate, which is the amount of data successfully transmitted to the DCN divided by the total amount of data transmitted from the NSNs, as a performance measure.

By connecting successive reconstructed images, video recordings can be produced to implement "invisible surveillance cameras." To achieve this, the NSNs should transmit their data periodically, and the DCN should be able to consistently reconstruct images each time the data transfer process is completed. For simplicity, the reconstruction time interval can be considered equivalent to the transmission period, which is denoted by $1/R_{\mathrm{I}}$. In this case, the frame rate, which is often used as a measure of video quality, is simply expressed as R_{I}. Increasing the frame rate enhances the video quality; however, to enable this under the proposed TL-TDA protocol, the transmission period needs to be shortened, which results in a decrease in capacity. In this paper, we discuss the proposed TL-TDA from the perspectives of application and communication.

III. Proposed MAC protocol suitable for periodic networked imaging

In this section, we describe the proposed TL-TDA protocol. Under this protocol, the NSNs are divided into several clusters, as shown in Fig. 1(b). Here, we assume small-area (80-cm-square) hexagonal clusters. The DCN is located at the center of the clusters, whereas the NSNs are randomly positioned among the clusters. Each NSN transfers data via a cluster head (CH) selected from among the NSNs located near the center of each cluster. The CHs aggregate the received data into a single packet and send them to the DCN. Each NSN has its own ID (NSN-ID), and the number of NSNs belonging to the i-th cluster is given by M_i, where $1 \leq i \leq H$, and H is the number of clusters. The example in Fig. 1(b) focuses on the case $H = 3$.

The data flow under TL-TDA is shown in Fig. 2. TL-TDA operates in two modes: coordinating and periodic imaging. In the coordinating mode, the periodic imaging and data transfer process is prepared by having the central station of the DCN assign fixed-length time-slots to each NSN and CH from the N_{L1} and N_{L2} time-slots in Layers 1 and 2, respectively. The assignment method is described in detail in Sec. III-A. After completion of the coordinating process, the periodic imaging mode begins, and following the transmission of a beacon packet from the DCN, each NSN captures a single-pixel image and sends it to the DCN via TL-TDA. The periodic imaging mode is described in detail in Sec. III-B. It is assumed that

each layer uses a different set of MHz-band frequencies for communication. Finally, the DCN reconstructs the image from the collected data. As noted earlier, the values of N_{L1} and N_{L2} depend strongly on the number of clusters and the frame rate. Because the time-slot duration in Layer 1 is fixed, the frame rate R_{I} determines the value N_{L1}, as shown in Fig. 2. Further, as a result of the aggregation process, the time-slot duration in Layer 2 is proportional to M_i. N_{L2} is a function of H because increasing H decreases M_i for a fixed M. A detailed analysis of these relationships is provided in Sec. IV.

The proposed TL-TDA has several intriguing features that can be used to obtain focused imaging applications. Owing to the use of centralized TDA, long headers and redundant times (such as contention windows), which often appear in ad hoc protocols, are not required. In fact, the header in the TL-TDA physical layer is only 18 bytes long. This header, which is often applied as the PLCP preamble under IEEE 802.11, is necessary for synchronization in the physical layer, and its size is significantly reduced relative to typical IEEE 802.11 CSMA/CA protocols, which require 54-byte headers. Furthermore, the clustering method employed under TL-TDA enables simultaneous the transmission between clusters. Consequently, these features significantly improve the network capacity and enable data transfer from thousands of NSNs. In addition, the use of TDA provides an additional benefit in terms of periodic imaging by guaranteeing a specific delivery time from the NSNs to the DCN. As shown in Fig. 2, after the NSNs capture their images, they periodically transmit packets during their assigned time slots; thus, only two periods are required to transfer the data to the DCN, which contributes to effective real-time video recording.

Moreover, MAC protocols based on TDA require time synchronization among nodes. Certain techniques for synchronization in nanoscale communications have been demonstrated, such as in [40]. In the field of ad hoc networks, a synchronization method was also proposed in [41]. In particular, the beacon-based adaptive time synchronization method for wireless sensor networks [42] is suitable for the proposed method because, as shown in Fig. 2, the DCN transmits the beacon as the timing packet at the beginning of the frame. In terms of the implementation, the procedures followed by the proposed TL-TDA protocol can be performed in LSI chips. If a small-sized chip is available, connecting the nanoscale RF front-end to the small LSI chip enables the realization of ultra-small sensor nodes.

A. Coordinating mode

The coordination mode was designed to obtain a unique assignment of time slots to the NSNs. Here, we focus on non-overlapping assignment in each cluster. In a manner similar to existing methods [36]–[38], under the proposed TL-TDA, the DCN assigns time slots by communicating from the NSNs to the DCN via TDA. Successful communication is required to carry out the assignment, and to achieve this, we exploit an appealing feature of the proposed system wherein each CH and NSN has a unique ID. Each NSN is assigned a unique random filter to obtain single-pixel data [31]. The ID of this filter can be treated as a CH- or NSN-ID, with each CH and NSN selecting the time slot for which the number matches its own ID. Unlike existing methods, TL-TDA allows thousands of NSNs to communicate with the DCN without collision.

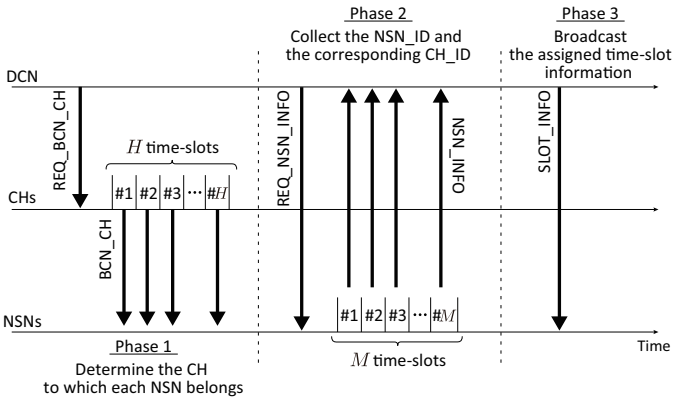

Fig. 3. Coordinating mode communication diagram. In the proposed system, CH-ID and NSN-ID are uniquely assigned. Exploiting this feature, each CH and NSN selects the time-slot with the number matching its own CH-ID or NSN-ID. This results in successful communication among all DCN, CHs, and NSNs requiring slot assignment.

The flow of the proposed slot assignment approach is shown in Fig. 3. In phase 1, each NSN determines the CH to which it belongs by identifying the CH closest to its location. The DCN first requests each CH to send a beacon packet by broadcasting a `REQ_BCN_CH` packet. After receiving this packet, each CH counts the time-slot number, and when it matches its own CH-ID, the CH broadcasts a `BCN_CH` packet containing the CH-ID. The NSNs listen to the packets to measure the received signal strength. Subsequently, each NSN ranks the CHs in order of the measured strength and selects the CH with the highest value as the one to which it belongs. This method for the selection of time slots based on the CH-ID avoids packet collisions among the CHs.

In phase 2, the DCN attempts to collect the information corresponding to the CH-ID selected by each NSNs; this information is necessary for achieving slot assignment at the DCN. The DCN broadcasts a beacon packet, `REQ_NSN_INFO`, to request the transmission of selected CH-IDs. In a manner similar to phase 1, after receiving this packet, each NSN counts the time-slot number, and when it matches its own NSN-ID, the NSN transmits the `NSN_INFO` packet that includes the selected CH-ID and its own NSN-ID.

After the DCN receives the `NSN_INFO` packets from each NSN, it uses the collected information to assign unique time slots to the NSNs in each cluster; these time slots are reused among the clusters. Finally, in phase 3, the DCN broadcasts the results of the slot assignment with a `SLOT_INFO` packet; upon receiving this packet, each NSN obtains its assigned time slot. Note that, if the number of NSNs in a cluster exceeds the number of time slots in Layer 1, that is, $M_i > N_{\mathrm{L1}}$, the DCN will not assign time slots to the excess NSNs, and thus, these NSNs cannot transmit their single-pixel data.

B. Periodic imaging mode

Once the coordinating mode is complete, periodic imaging begins. As shown in Fig. 2, the DCN first periodically broadcasts a beacon packet to instruct the NSNs on how to time the capturing of single-pixel images. Following image capture, each NSN prepares for transmission and sends its captured image to its CH during the assigned time slot in the lower layer of Layer 1. Subsequently, the CH aggregates the received data into a single packet and, in the upper layer of Layer 2, sends the packet to the DCN. Thereafter, the DCN collects the data from all NSNs and reconstructs the images.

The number of clusters, H, is a key parameter that indicates the capacity of the proposed TL-TDA protocol. As shown in Fig. 1(b), for a fixed total number of NSNs M, H determines the average number of NSNs per cluster, namely, $\lceil M/H \rceil$. Note that $\lceil \cdot \rceil$ is a ceiling function, and to support communication from all NSNs, this number should be sufficiently smaller than the number of time-slots, N_{L1}, which is determined by the frame rate R_{I}. When H increases, this condition is easily satisfied; however, the number of CHs, reflecting the number of aggregated packets transmitted in Layer 2, also increases. If the number of CHs exceeds N_{L2}, a lack of capacity arises, leading to the non-delivery of data from the CHs to the DCN. A theoretical analysis in terms of network capacity is presented in the following section.

IV. Theoretical Design of Clustering Structure for Periodic Imaging Application

In this section, we present a design framework for a clustering structure to establish the proposed periodic imaging application. As discussed earlier, a higher frame rate corresponds to an improved video quality from periodic imaging. However, as discussed in Sec. III-B, an excessively high frame rate can lead to data transfer failure. Therefore, to balance these factors, we theoretically derive the optimal number of clusters to achieve the maximum frame rate.

One of the key techniques applied by the proposed TL-TDA approach is data aggregation at the CHs. For this method to work effectively, the total amount of data received by the CHs should be equal to or smaller than the amount of data that can be sent in Layer 2. Otherwise, a part of the received data will not be included in the aggregated packet, and the residual data must be stacked at the CHs or discarded. To assess this situation, we introduce the concept of achievable data-collection rate (ADCR) to describe the maximum frequency of successful receptions at the CHs and DCN during one period, $1/R_{\mathrm{I}}$. This rate is strongly correlated with the maximum frame rate that is to be derived; for example, the ADCR in Layer 2, which is denoted by R_{L2}, equals the maximum frequency at which the single-pixel data are delivered to the DCN and reconstruction is performed. The Layer 1 ADCR, denoted by R_{L1}, indicates the rate at which the CHs receive data from the NSNs. Therefore, to avoid the stacked situation described above, these two ADCRs must satisfy the condition $|R_{\mathrm{L1}} - R_{\mathrm{L2}}| \simeq 0$. This condition provides the optimal frame rate, denoted by $R_{\mathrm{I_{opt}}}$, as follows:

$$R_{\mathrm{I_{opt}}} = \min_{H \in \mathbb{N}} \left[|R_{\mathrm{L1}} - R_{\mathrm{L2}}| \right]. \tag{1}$$

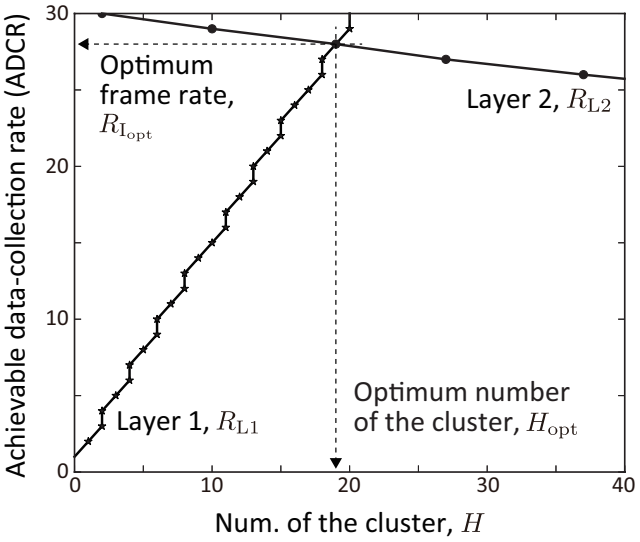

Fig. 4. Example of achievable data-collection rate (ADCR) as a function of number of clusters, H. The optimal frame rate and corresponding optimal number of clusters are obtained according to (1). This figure corresponds to the cases: $L = 27$ bits, $M = 4096$, $T_{\mathrm{s}} = 144\,\mu$s, $B_{\mathrm{L1}} = 1.0$ Mbps and $B_{\mathrm{L2}} = 3.0$ Mbps.

Thus, the optimal number of clusters, denoted by H_{opt}, is the value that satisfies (1). In the following, we derive R_{L1} and R_{L2}.

The ADCR in Layer 1 is derived by calculating the number of time slots. In this layer, NSNs send data packets with a fixed size of $L = 24$ bits and a bandwidth of B_{L1}. Considering that a time interval of T_{s} is required prior to transmission to achieve synchronization in the physical layer via, for instance, the PLCP preamble, the required time for transmitting data is $T_{\mathrm{s}} + L/B_{\mathrm{L1}}$. Further, the ADCR in this layer is obtained for the case in which one period is fully occupied by the transmitted packets from all of the NSNs in a cluster. Mathematically, $N_{\mathrm{L1}} \approx \lceil M/H \rceil$ because there are, on average, M NSNs in H clusters; therefore, the total transmission time is $(T_{\mathrm{s}} + L/B_{\mathrm{L1}})\lceil M/H \rceil$. Thus, the ADCR in Layer 1 equals the inverse of the total time:

$$R_{\mathrm{L1}} = \left\{ \left(T_{\mathrm{s}} + \frac{L}{B_{\mathrm{L1}}} \right) \left\lceil \frac{M}{H} \right\rceil \right\}^{-1}. \tag{2}$$

In Layer 2, CHs transmit aggregated data to the DCN. The amount of data sent by a CH is $L\lceil M/H \rceil$, which corresponds to an aggregated packet duration of $T_{\mathrm{s}} + L\lceil M/H \rceil / B_{\mathrm{L2}}$. Because there are H CHs, that is, $N_{\mathrm{L2}} = H$, the total time for the transmission of aggregated packets from all CHs is $H(T_{\mathrm{s}} + L\lceil M/H \rceil / B_{\mathrm{L2}})$. Thus, the ADCR in Layer 2 can be expressed as

$$R_{\mathrm{L2}} = \left\{ \left(T_{\mathrm{s}} + \frac{L}{B_{\mathrm{L2}}} \left\lceil \frac{M}{H} \right\rceil \right) H \right\}^{-1}. \tag{3}$$

Numerical examples of ADCRs and the optimal number of clusters are presented in Fig. 4. Here, we focus on the case $M = 4096$. According to [43], $T_{\mathrm{s}} = 144\,\mu$s, $B_{\mathrm{L1}} = 1.0$ Mbps, and $B_{\mathrm{L2}} = 3.0$ Mbps. To enable the detection of erroneous transmissions, three parity bits are added to the single-pixel

data, resulting in $L = 27$ bits. As shown in Fig. 4, the ADCR values depend on the number of clusters. In Layer 1, decreasing H increases the required time for transmission from all NSNs in a cluster. This is reflected in (2), wherein the number of nodes per cluster depends on the number of clusters, that is, $\lceil M/H \rceil$. Thus, decreasing H results in a decrease in the ADCR of Layer 1. By contrast, in Layer 2, the ADCR decreases slightly as H increases, as in this case, many aggregated packets can be transmitted from the CHs. As indicated by (3), each packet has a required transmission time of $T_{\rm s}$; increasing the number of clusters increases the length of this redundant time, which consequently increases the header size relative to the amount of data and results in a lack of capacity.

The two curves in Fig. 4 cross at a specific number of clusters; this point represents the optimal frame rate and the corresponding optimal number of clusters. As the number of clusters increases beyond this point, the ADCR in Layer 1 can increase, but the header size in Layer 2 also increases, reducing the number of aggregated packets that can be transmitted in each period. This results in a decrease in the ADCR in Layer 2. By contrast, if the number of clusters is smaller than $H_{\rm opt}$, there will be a smaller number of aggregated packets to be transmitted; however, the amount of single-pixel data to be transmitted in Layer 1 will exceed the capacity of that layer, resulting in missed transmissions. Thus, (1) provides the optimal number of clusters under the current settings: $H_{\rm opt} = 19$ and $R_{\rm I_{opt}} = 28$. The analysis in this section did not consider packet collision or errors in data transfer, that is, the reception rate was assumed to be equal to 100%. However, in practice, demodulation errors and packet collisions lead to a decrease in the reception rate and imperfect data transfer, which reduces the quality of the transmitted images. In the next section, we discuss the influence of the reception rate in our demonstration of the periodic imaging approach.

System latency is an important metric that should be considered when designing the proposed TL-TDA protocol. In periodic imaging, we should consider the additional time interval to avoid the influence of latency; if such an interval exists in the timing chart shown in Fig. 2, the bandwidth used for the data transfer is reduced, resulting in the reduction of the frame rate or the ADCR. This influence can be considered with the term $T_{\rm s}$. Such an additional time can be considered as a part of $T_{\rm s}$; the extension of this term leads to a small value of the ADCR. Note that in the proposed coordinating mode, as shown in Fig. 3, slot assignment is executed in a handshaking manner among the DCN, CHs, and NSNs. However, if latency exists, receiving the response from the surrounding nodes require additional time, which results in the extension of the required time to complete the slot assignment procedure.

V. Demonstration of Periodic Networked Imaging using the Proposed TL-TDA Protocol

Here, we demonstrate the proposed method for periodic imaging via spatially distributed NSNs using the TL-TDA protocol. The demonstration scenario and parameter setup are described in Sec. V-A. A discussion on the communication behavior is provided in Sec. V-B, which provides numerical results with respect to the reception rate. The main results corresponding to the obtained images are presented in Sec. V-C.

A. Demonstration scenario and parameter setup

As NSN is currently under development, to perform this demonstration, we emulated the periodic imaging application by evaluating the reconstruction of a pre-recorded video. The coordinating mode was assumed to have been completed, and the periodic imaging mode was simulated on a computer. The video was divided into images of size 96×96 pixels and, according to [31], each image was converted into single-pixel data. The NSNs were randomly positioned, based on the outline shown in Fig. 1(b). They transmitted data using the proposed TL-TDA in which the protocol parameters— M, $B_{\rm L1}$, $B_{\rm L2}$, L, and $T_{\rm s}$—were the same as those described in Sec. IV. In this case, the time-slot duration in Layer 1 was fixed at 171 μs. In addition, as discussed in Sec. IV, the duration in Layer 2 varied according to the number of NSNs per cluster. At the DCN, the images were reconstructed using the received data. However, when the data transfer failed, a portion of the transmitted single-pixel data could not reach the DCN and the images were reconstructed using an imperfect dataset. To reflect this in the simulation, the original single-pixel data were randomly extracted in accordance with the reception rate and used in the reconstruction. Note that the time slots were assumed to be synchronized among the nodes.

Signal propagation and the behavior in the physical layer should be considered to simulate data transfer using the proposed method via a wireless link. We attempted to perform the demonstration using a simple model wherein the transmitted signal power was sufficiently strong to avoid the occurrence of demodulation errors in the physical layer of the CHs and DCN. However, packet collision may occur, and hence data transfer may fail, as signals from NSNs located near the cluster borders could easily reach the CHs of neighboring clusters. In such circumstances, it is possible for two NSNs belonging to different clusters to transmit using the same time slot. According to the capture effect [44]–[46], when there is an identifiable difference in the power received from both NSNs, the packet with the larger amount of power is successfully received, while the other is lost. In this demonstration, the received power ratio, which was calculated based on the position of the NSNs according to a free-space propagation loss model for MHz-band signaling, was set to 5.0 dB.

B. Communication performance numerical results

Before demonstrating the periodic imaging approach, we evaluate the communication performance of the proposed TL-TDA protocol. As discussed in Sec. II, we focus on the reception rate in this evaluation. For the scenario described in Sec. V-A, the received signal power was calculated based on the node positions, and subsequently, the packet collision rate was evaluated based on this. These calculations were repeated 1,000 times with the node positions shown in Fig. 1(b) being randomly varied, and the resulting average reception rates for the TL-TDA were evaluated; these are shown in Fig. 5(a),

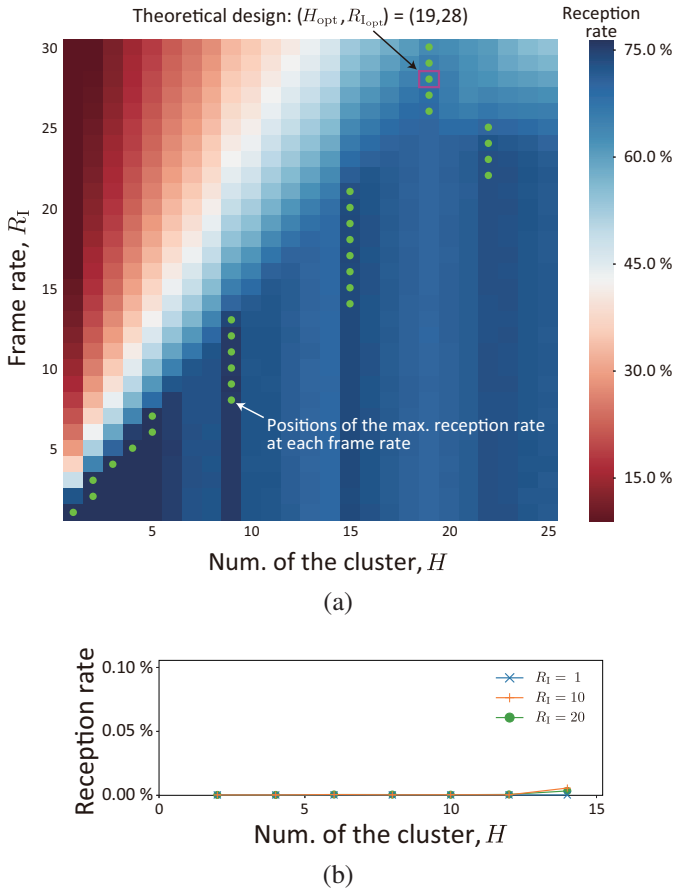

Fig. 5. Numerical example of reception rate in (a) the proposed method (TL-TDA) and (b) IEEE 802.11e PCF mode. In the proposed method, the reception rate varies significantly depending on the number of clusters and the frame rate. The maxima in terms of number of clusters at each frame rate are marked by green circles. The reception rates at these positions are provided in Fig. 6. The magenta rectangle marks the theoretically derived optimum number of clusters, $H_{\rm opt}$, and the corresponding frame rate, $R_{\rm I_{opt}}$. Unlike the proposed method, the existing method of IEEE 802.11e PCF mode provides a poor reception rate regardless of the number of the cluster and frame rate.

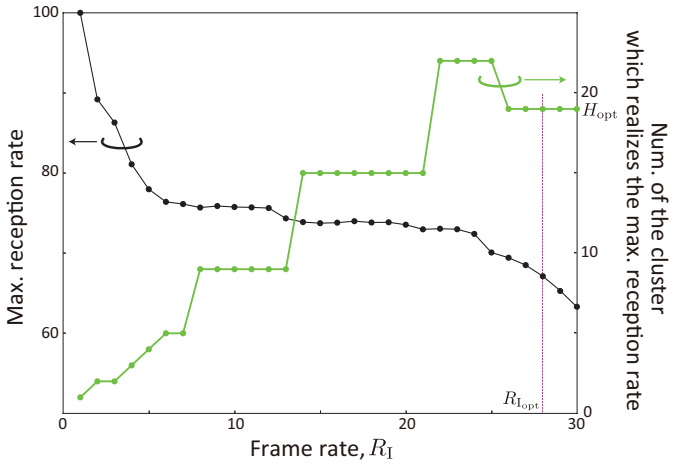

Fig. 6. Reception rate as a function of frame rate. The maximum rate is shown as the black curve. As the frame rate increases, the maximum gradually decreases. The number of clusters that produce each maximum are shown as the green curve. At the optimal $H_{\rm opt}$, more packets fail to transfer than in cases with smaller frame rates. This indicates that smaller cluster numbers can provide images of suitable quality, as is discussed in Sec. V-C.

wherein the average values can be determined from the color. The dependence of the average rate on the number of clusters and the frame rate can be observed in this figure. However, in all parameter ranges, the reception rate is far less than 100%, and data transfer often fails. This is particularly true in the red-colored region, wherein the reception rate is significantly reduced. In this situation, corresponding to a reduced number of clusters, the number of time slots is often smaller than the number of NSNs, M_i, resulting in a condition wherein the time slots cannot be uniquely assigned to all the NSNs. This results in a lack of capacity because some packets cannot be transmitted in Layer 1. By contrast, in the blue-colored region where a sufficient number of clusters exist, non-overlapped time slots can be assigned to the NSNs, which contributes significantly to improving both the reception rate and capacity.

Even when there is a sufficient number of clusters, some packet collisions are bound to occur and, as a result, the reception rate does not exceed 75%, as indicated by the blue region in Fig. 5(a). As discussed in Sec.V-A, colliding packets are transmitted from NSNs located in the vicinity of cluster edges. This degradation can potentially become serious as the number of clusters increases, as this increase the probability that NSNs will be located close to the edge areas.

An interesting behavior is observed in Fig. 5(a), wherein the maximum reception rate at each frame rate is found at a specific number of clusters. The green circles in the figure show the positions at which maxima are obtained. These maxima appear because a small number of clusters leads to a lack of capacity and a reduction in the reception rate. Although increasing the number of clusters improves this rate, beyond the green points, the rate decreases as a result of packet collision. The values of the maxima and the corresponding numbers of clusters are presented in Fig. 6. In the current setting, the theoretical design method introduced in Sec. IV derives the following optimal condition: $(H_{\rm opt}, R_{\rm I_{opt}}) = (19, 28)$. This setting is valid in terms of maximizing the frame rate; however, as shown in Fig. 6, the reception rate is deteriorated relative to cases with smaller numbers of clusters. In this case as well, packets transmitted from NSNs located at the edges of clusters can easily collide; however, the derivation in Sec. IV does not consider this situation. This reduction can affect the quality of the reconstructed image and, to avoid it, a slightly decreased cluster number, for example, $H \approx 20$, may be preferable. In Sec. V-C, we will further discuss this issue by evaluating the PSNRs of reconstructed images.

We compared the proposed TL-TDA with a similar method that exploits the point coordination function (PCF) standardized under IEEE802.11e [43], [47], [48]. This method is a TDA-like protocol in which transmission timing (slot assignment) for data transfer is coordinated under the PCF framework; before the transfer, the timing is determined in a polling manner with CSMA/CA. We evaluated this method by applying Network Simulator 3 (NS3) [49] with a simple method, CSMA/CA, implemented in Layer 2. The numerical results are presented in Fig. 5(b). Even at a low frame rate of $R_{\rm I} = 1.0$ and a large number of clusters, $H = 14$, the reception

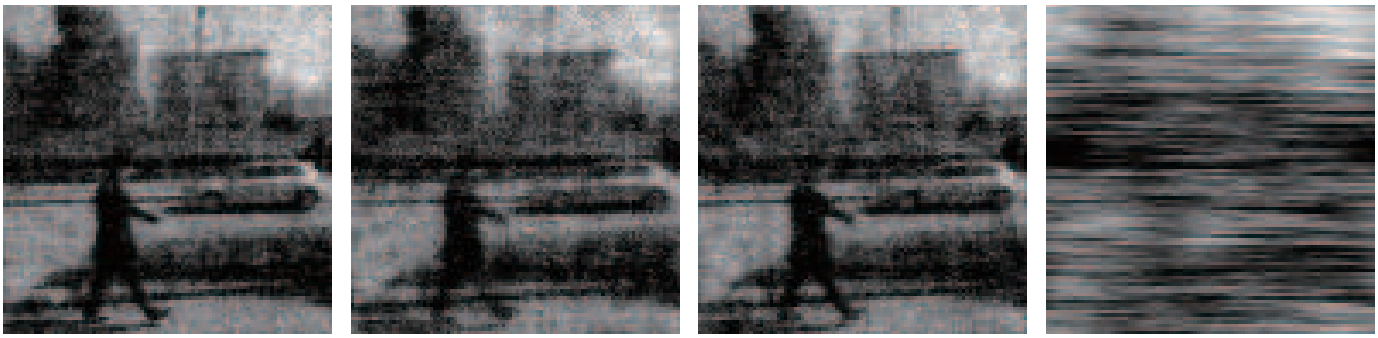

(a) (b) (c) (d)

Fig. 7. Results of periodic imaging using the proposed TL-TDA protocol. (a) Reconstructed image in the ideal case in which all single-pixel data successfully transfer to the DCN, that is, there are no transfer errors. To demonstrate an imaging application using the proposed TL-TDA, reconstructed images obtained using TL-TDA with a theoretical design, i.e., $(H_{\rm opt}, R_{\rm I_{opt}}) = (19, 28)$ are presented in (b). As discussed in Sec. V-B, under this design framework the reception rate is somewhat decreased; a slightly decreased number of clusters can produce a clearer image. To confirm this, a reconstructed image with $(H, R_{\rm I}) = (15, 20)$ is presented in (c). To demonstrate the effectiveness of employing the clustering method, (d) shows a reconstructed image obtained using single-pixel data transferred via TL-TDA without clustering, i.e., $(H, R_{\rm I}) = (1, 20)$. The quality of the obtained images, measured in terms of the PSNR, are: (a) 18.45 (b) 17.45 , (c) 17.78 , and (d) 13.96 dB.

rate was poor, 0.00312 %, which indicates that nearly all of the data transmission failed. This significant deterioration is due to the failure of the PCF. The slot assignment requests from many NSNs fail because the use of redundant time intervals and long headers in CSMA/CA communication significantly restricts the number of accessible NSNs during the polling.

C. Quality of reconstructed image examples

Several imaging results obtained using the proposed TL-TDA protocol are shown in Fig. 7. Figure 7(a) is a reconstructed image obtained under the ideal case wherein all of the single-pixel data are successfully transferred to the DCN, that is, there are no transfer errors. In this case, a high PSNR of 18.45 dB was obtained. In this image, a pedestrian walking along a street and a vehicle are clearly visible. A reconstructed image obtained using the proposed TL-TDA protocol with the theoretical design $(H_{\rm opt}, R_{\rm I_{opt}}) = (19, 28)$ is shown in Fig. 7(b). Relative to the image in Fig. 7(a), this image contains more darkish noise, and the PSNR is reduced to 17.45 dB. As predicted in Sec. V-B, under the theoretical design, data transfer may fail occasionally, resulting in a lack of the single-pixel data needed for reconstruction. To avoid this issue, a slightly decreased number of clusters can, in some cases, provide an image with better clarity. To confirm this, a reconstructed image with $(H, R_{\rm I}) = (15, 20)$ is shown in Fig. 7(c). In this image, the silhouettes of the pedestrian, vehicle, and building can be clearly distinguished; furthermore, the PSNR is improved to 17.78 dB.

To assess the effectiveness of employing the clustering method under the proposed TL-TDA, a reconstructed image obtained without clustering, that is, $(H, R_{\rm I}) = (1, 20)$, is shown in Fig. 7(d). In contrast to the other images, it contains no identifiable objects, and the PSNR is reduced significantly to 13.96 dB. These results arise from the small data transfer capacity of the reconstruction. In this case, only 297 time slots could be assigned to 4,096 NSNs. As most of the NSNs could not be assigned unique time slots, the data transfer often failed, as shown in Fig. 5, and the DCN was able to collect very little data from the NSNs. This resulted in a lack of data for reconstruction, and a reconstructed image with a significantly deteriorated quality was obtained. By contrast, when constructing the other images, there were sufficiently large numbers of clusters, which fully contributed to the successful transfer of single-pixel data to the DCN and produced reconstructed images with excellent quality.

We also evaluated the imaging results obtained for a number of videos, which are provided in the supplementary materials[1]. Each video was produced by connecting successive reconstructed images. The motion of the pedestrian and running vehicle can be observed in all of the videos except for the case without clustering. In addition, the clarity of the respective videos depends on the frame rate. As discussed earlier, data transfer at a lower frame rate results in clearer images but less smooth motion. To increase smoothness, the frame rate can be increased; however, as discussed in Sec. III, this decreases the number of time slots, which leads to data transfer failure, resulting in a lack of data for the reconstruction and a degraded image quality. Therefore, it is necessary to design the transfer parameters considering both the image quality and frame rate.

We note that the existing methods, such as the IEEE 802.11e PCF mode, do not provide good quality in periodic imaging. We reconstructed the image via PCF communication, and the resulting image was nearly black and had a very low PSNR of 6.30 dB. Figure 5(b) shows that most of the data transfer from the NSNs failed. Consequently, owing to the lack of single-pixel data, the reconstruction was not successful.

[1]The file "`ideal.avi`" contains a video produced by connecting the reconstructed images obtained under the ideal case, corresponding to the results shown in Fig. 7(a). The video for the optimal-setting image, shown in Fig. 7(b), is contained in the file "`theoretical.avi`". For comparison, we also created a video, "`H_15.avi`," for the condition $(H, R_{\rm I}) = (15, 20)$, which corresponds to the case shown in Fig. 7(c). Finally, the video "`without_clustering.avi`" was created without clustering in a manner similar to the image in Fig. 7(d).

VI. Related works on NSN communications

In this section, we discuss communication techniques related to NSNs in the context of nano communication. Such techniques can be classified into three major categories in terms of the communication medium: molecular, electromagnetic-based THz-band, and electromagnetic-based MHz-band communications [3], [20]. In this study, electromagnetic-based communication was focused on as a means of achieving data transfer between physically distant nodes.

Previous investigations have examined the use of THz-band communication electromagnetic signaling for nanoscale devices [50]–[54]. THz-band wavelengths are quite short, which makes the antenna size suitable for nanoscale devices, and a number of MAC protocols for this frequency range have been proposed [52]–[54]. However, such signals are strongly attenuated in the propagation phase, and designing electric circuits for this band is difficult and costly. To overcome these drawbacks, the use of MHz-band signaling with nanomechanical systems has been investigated [12]–[15], [17].

Standard MAC protocols such as CSMA/CA, which is used under IEEE 802.11, appear to be the most likely candidates for communication in the MHz-band [43], [55]–[57]. However, to avoid packet collision, they require redundant times with random backoffs, in addition to long packet headers. Moreover, to transmit small amounts of single-pixel data, a very large MAC header size is required in these methods. This implies that most of the time required to send a packet is occupied by the header and redundant times, which results in a shortage of capacity and, therefore, a significant decrease in the number of covered NSNs. Based on these considerations, the existing CSMA/CA-based MAC protocols are unsuitable for handling communication from thousands of NSNs.

The lack of communication capacity in CSMA/CA-based access has a serious impact on TDA access. TDMA-based MAC protocols have also been investigated in the field of wireless sensor networking (e.g., [22], [32]–[39], [58]–[60]). S-MAC [37] introduced periodic listen and sleep to decrease power consumption. Z-MAC [38] is a hybrid of CSMA/CA and TDMA, which has a frame contention function from introducing two priority modes. Inherently, TDA-based methods require slot assignments to determine the timing of communication. However, in the aforementioned approaches, CSMA/CA is primarily used for slot assignment. Owing to the lack of communication capacity, requests for slot assignment cannot reach the DCN; thus, all nodes do not obtain an opportunity to transmit their data. Certain interesting optimal scheduling methods [58]–[60] also do not consider a large-scale sensor network, as shown in Fig. 1. To overcome the drawbacks of these methods, we propose efficient slot assignment by utilizing NSN-ID and a handshaking process. In wireless sensor networks, the clustering method has often been introduced to shorten the transmission distances; examples are found in [22], [61]. Such a method is effective from the perspective of header reduction. In [61], another critical issue of suppressing power consumption was discussed; however, the suppression procedure requires redundancy to accommodate numerous nodes, which cannot support large-scale networks.

Another TDA-like protocol involves the use of PCF under IEEE802.11e with a hybrid coordination function (HCF)-controlled channel access (HCCA) [43], [47], [48]. However, as discussed in Sec. V-B, the failure of PCF to add to the polling list results in erroneous data transfer. Thus, overall, the existing MAC protocols are inadequate for handling communication among a large number of NSNs.

VII. Conclusion

As a step toward the future application of invisible video monitoring systems, in this paper, we present a communication framework involving a large number of NSNs. Under the proposed MAC protocol, TDA is applied to reduce redundant headers, which significantly improves the transmission capacity. The introduction of a two-layered protocol enables simultaneous transmission between clusters, which enhances network capacity. Further, in contrast to existing methods, the proposed method does not require CSMA/CA-based access in the slot assignment process. The results of the numerical simulation revealed that the proposed TL-TDA protocol enables periodic imaging applications with more than three thousand nodes. Moreover, using the proposed TL-TDA, images with quality similar to those of ideal communication images were obtained. The capability of the proposed method is ensured through a design framework for determining the key parameters of the number of clusters and the frame rate. Although NSN technology is still under development, we believe that the proposed method will contribute to IoNT in the near future.

In this study, we focused on a nanomechanical-based wireless communication technique. Exploiting a nanomechanical vibration, we can use MHz-band signaling even in the case of the small size of invisible sensor nodes. Similar to the existing methods, one can focus on THz-band signaling; however, the communication range is limited in this case. To cover all NSNs in such a situation, the area of the cluster should be designed to be small. This is achieved by increasing the number of clusters, H; however, as shown in Figs. 4 and 5, the ADCR and reception rate decrease. Thus, to maintain a high performance in both communication and imaging, the number of clusters should be carefully designed according to the channel model.

References

[1] J. Lin, W. Yu, N. Zhang, X. Yang, H. Zhang, and W. Zhao, "A Survey on Internet of Things: Architecture, Enabling Technologies, Security and Privacy, and Applications," *IEEE Internet Things J.*, vol. 4, no. 5, pp. 1125–1142, Oct. 2017.

[2] A. Al-Fuqaha, M. Guizani, M. Mohammadi, M. Aledhari, and M. Ayyash, "Internet of Things: A Survey on Enabling Technologies, Protocols, and Applications," *IEEE Commun. Surveys Tuts.*, vol. 17, no. 4, pp. 2347–2376, 4th Quart. 2015.

[3] G. Gardašević, M. Veletić, N. Maletić, D. Vasiljević, I. Radusinović, S. Tomović, and M. Radonjić, "The IoT Architectural Framework, Design Issues and Application Domains," *Wireless Pers. Commun.*, vol. 92, no. 1, pp. 127–148, Oct. 2017.

[4] S. M. R. Islam, D. Kwak, M. H. Kabir, M. Hossain, and K. Kwak, "The Internet of Things for Health Care: A Comprehensive Survey," *IEEE Access*, vol. 3, pp. 678–708, Jun. 2015.

[5] H. Habibzadeh, K. Dinesh, O. R. Shishvan, A. Boggio-Dandry, G. Sharma, and T. Soyata, "A Survey of Healthcare Internet of Things (HIoT): A Clinical Perspective," *IEEE Internet Things J.*, vol. 7, no. 1, pp. 53–71, Jan. 2020.

[6] A. Zanella, N. Bui, A. Castellani, L. Vangelista, and M. Zorzi, "Internet of Things for Smart Cities," *IEEE Internet Things J.*, vol. 1, no. 1, pp. 22–32, Feb. 2014.

[7] K. Eom, H. S. Park, D. S. Yoon, and T. Kown, "Nanomechanical resonators and their applications in biological/chemical detection: nanomechanics principles," *Phys. Rep.*, vol. 503, no. 4, pp. 115-–163, Jun. 2011.

[8] P. M. Kosaka, V. Pini, J. J. Ruz, R. A. da Silva, M. U. González, D. Ramos, M. Calleja, and J. Tamayo, "Detection of cancer biomarkers in serum using a hybrid mechanical and optoplasmonic nanosensor," *Nat. Nanotech.*, vol. 9, no. 12, pp. 1047-–1053, Nov. 2014.

[9] V. Puller, B. Lounis, and F. Pistolesi, "Single molecule detection of nanomechanical motion," *Phys. Rev. Lett.*, vol. 110, no. 12, p. 125501, Mar. 2013.

[10] J. Chaste, A. Eichler, J. Moser, G. Ceballos, R. Rurali, and A. Bachtold, "A nanomechanical mass sensor with yoctogram resolution," *Nat. Nanotech.*, vol. 7, pp. 301-–304, Apr. 2012.

[11] J. Lee, W. Shen, K. Payer, T. P. Burg, and S. R. Manalis, "Toward attogram mass measurements in solution with suspended nanochannel resonators," *Nano Lett.*, vol. 10, no. 7, pp. 2537-–2542, Jul. 2010.

[12] B. Atakan and O. Akan, "Carbon nanotube-based nanoscale ad hoc networks," *IEEE Commun. Mag.*, vol. 48, no. 6, pp. 129–135, Jun. 2010.

[13] K. Jensen, J. Weldon, H. Garcia, and A. Zettl, "Nanotube Radio," *Nano Lett.*, vol. 7, no. 11, pp. 3508–3511, Nov. 2007.

[14] V. Gouttenoire, T. Barois, S. Perisanu, J.-L. Leclercq, S. T. Purcell, P. Vincent, and A. Ayari, "Digital and FM Demodulation of a Doubly Clamped Single-Walled Carbon-Nanotube Oscillator: Towards a Nanotube Cell Phone," *Small*, vol. 6, no. 9, pp. 1060–1065, May 2010.

[15] C. E. Koksal and E. Ekici, "Applications and performance of a nanoreceiver with a carbon nanotube antenna forest," *IEEE Wireless Commun.*, vol. 19, no. 5, pp. 52–57, Oct. 2012.

[16] T. Nan et al., "Acoustically actuated ultra-compact NEMS magnetoelectric antennas," *Nat. Commun.*, vol. 8, no. 1, p. 296, Aug. 2017.

[17] Y. Tadokoro, H. Tanaka, and M. I. Dykman, "Driven nonlinear nanomechanical resonators as digital signal detectors," *Sci. Rep.*, vol. 8, p. 11284, Jul. 2018.

[18] H. Tanaka, Y. Ohno, and Y. Tadokoro, "Adaptive control of angular sensitivity for VHF-band nanoantenna using CNT mechanical resonator," *IEEE Trans. Mol. Biol. Multi-Scale Commun.*, vol. 3, no. 1, pp. 24–32, Mar. 2017.

[19] Y. Ito, K. Funayama, J. Hirotani, Y. Ohno, and Y. Tadokoro, "Stochastic Optimal Control to Minimize the Impact of Manufacturing Variations on Nanomechanical Systems," *IEEE Access*, vol. 7, pp. 171195-–171205, Nov. 2019.

[20] I. F. Akyildiz, F. Brunetti, and C. Blázquez, "Nanonetworks: a new communication paradigm," *Comput. Networks*, vol. 52, no. 12, pp. 2260–2279, Aug. 2008.

[21] F. Peper, K. Leibnitz, J. Teramae, T. Shimokawa, and N. Wakamiya, "Low-Complexity Nanosensor Networking Through Spike-Encoded Signaling," *IEEE Internet Things J.*, vol. 3, no. 1, pp. 49–58, Feb. 2016.

[22] S. Canovas-Carrasco, R. M. Sandoval, A. Garcia-Sanchez, and J. Garcia-Haro, "Optimal Transmission Policy Derivation for IoNT Flow-Guided Nano-Sensor Networks," *IEEE Internet Things J.*, vol. 6, no. 2, pp. 2288–2298, Apr. 2019.

[23] L. Feng, Q. Yang, D. Park, and K. S. Kwak, "Energy Efficient Nano-Node Association and Resource Allocation for Hierarchical Nano-Communication Networks," *IEEE Trans. Mol. Biol. Multi-Scale Commun.*, vol. 4, no. 4, pp. 208–220, Dec. 2018.

[24] P. K. D. Pramanik, A. Solanki, A. Debnath, A. Nayyar, S. El-Sappagh, and K. Kwak, "Advancing Modern Healthcare With Nanotechnology, Nanobiosensors, and Internet of Nano Things: Taxonomies, Applications, Architecture, and Challenges," *IEEE Access*, vol. 8, pp. 65230–65266, Apr. 2020.

[25] E. Dinc and O. B. Akan, "Theoretical Limits on Multiuser Molecular Communication in Internet of Nano-Bio Things," *IEEE Trans. Nanobiosci.*, vol. 16, no. 4, pp. 266–270, Apr. 2017.

[26] Y. A. Qadri, A. Nauman, Y. B. Zikria, A. V. Vasilakos, and S. W. Kim, "The Future of Healthcare Internet of Things: A Survey of Emerging Technologies," *IEEE Commun. Surveys Tuts.*, vol. 22, no. 2, pp. 1121–1167, Feb. 2020.

[27] S. Canovas-Carrasco, R. Asorey-Cacheda, A. J. Garcia-Sanchez, J. Garcia-Haro, K. Wojcik, and P. Kulakowski, "Understanding the Applicability of Terahertz Flow-Guided Nano-Networks for Medical Applications," *IEEE Access*, vol. 8, pp. 214224–214239, Nov. 2020.

[28] S. Balasubramaniam and J. Kangasharju, "Realizing the Internet of Nano Things: Challenges, Solutions, and Applications," *Computer*, vol. 46, no. 2, pp. 62–68, Feb. 2013.

[29] D. Seo et al., "Wireless Recording in the Peripheral Nervous System with Ultrasonic Neural Dust," *Neuron*, vol. 91, no. 3, pp. 529–539, Aug. 2016.

[30] M. H. Ghaed et al., "Circuits for a Cubic-Millimeter Energy-Autonomous Wireless Intraocular Pressure Monitor," *IEEE Trans. Circuits Syst. I, Reg. Papers*, vol. 60, no. 12, pp. 3152–3162, Dec. 2013.

[31] T. Nobunaga, H. Tanaka, and Y. Tadokoro, "Reconstruction for spatially distributed single-pixel imaging based on pattern filtering," *IEEE Signal Process Lett.*, vol. 25, no. 5, pp. 705–709, May 2018.

[32] Y. Wang, I. Henning, X. Li, and D. Hunter, "SOTP: A Self-Organized TDMA Protocol for Wireless Sensor Networks," in *2006 Canadian Conference on Electrical and Computer Engineering*, pp. 1108–1111, 2006.

[33] W. L. Lee, A. Datta, and R. Cardell-Oliver, "FlexiTP: A Flexible-Schedule-Based TDMA Protocol for Fault-Tolerant and Energy-Efficient Wireless Sensor Networks," *IEEE Trans. Parallel Distrib. Syst.*, vol. 19, no. 6, pp. 851–864, Jun. 2008.

[34] T. Hsu and P. Yen, "Adaptive time division multiple access-based medium access control protocol for energy conserving and data transmission in wireless sensor networks," *IET Commun.*, vol. 5, no. 18, pp. 2662–2672, Dec. 2011.

[35] D. Buranapanichkit and Y. Andreopoulos, "Distributed Time-Frequency Division Multiple Access Protocol for Wireless Sensor Networks," *IEEE Wireless Commun. Lett.*, vol. 1, no. 5, pp. 440–443, Oct. 2012.

[36] W. B. Heinzelman, A. P. Chandrakasan, and H. Balakrishnan, "An application-specific protocol architecture for wireless microsensor networks," *IEEE Trans. Wireless Commun.*, vol. 1, no. 4, pp. 660–670, Oct. 2002.

[37] Y. Wei, J. Heidemann, and D. Estrin, "Medium access control with coordinated adaptive sleeping for wireless sensor networks," *IEEE/ACM Trans. Netw.*, vol. 12, no. 3, pp. 493–506, Jun. 2004.

[38] I. Rhee, A. Warrier, M. Aia, J. Min, and M. L. Sichitiu, "Z-MAC: A Hybrid MAC for Wireless Sensor Networks," *IEEE/ACM Trans. Netw.*, vol. 16, no. 3, pp. 511–524, Jun. 2008.

[39] P. Engelhard, A. Zachlod, J. Schulz-Zander, and S. Du, "Toward scalable and virtualized massive wireless sensor networks," in *2019 International Conference on Networked Systems (NetSys)*, pp. 1-6, Mar. 2019.

[40] P. Singh, B. W. Kim, and S. Y. Jung, "Preamble-based synchronisation scheme for electromagnetic wireless nanocommunications," *IET Commun.*, vol. 11, no. 7, pp. 1097–1105, Apr. 2017.

[41] H. Tanaka, O. Masugata, D. Ohta, A. Hasegawa, and P. Davis, "Fast, self-adaptive timing-synchronisation algorithm for 802.11 MANET," *Electron. Lett.*, vol. 42, no. 16, pp. 932–933, Aug. 2006.

[42] J. He, X. Xuan, N. Zhu, N. Huang, and P. He, "Mobile beacon-based adaptive time synchronization for wireless sensor networks," *J. Wireless Com. Network.*, vol. 2018, no. 1, p. 220, Sep. 2018.

[43] B. O'Hara and A. Petrick, IEEE 802.11 Handbook: A Designer's Companion. 2005, p. 404.

[44] K. J. Hyun and L. J. Kyu, "Capture effects of wireless CSMA/CA protocols in Rayleigh and shadow fading channels," *IEEE Trans. Veh. Technol.*, vol. 48, no. 4, pp. 1277–1286, Jul. 1999.

[45] F. Daneshgaran, M. Laddomada, F. Mesiti, M. Mondin, and M. Zanolo, "Saturation throughput analysis of IEEE 802.11 in the presence of non ideal transmission channel and capture effects," *IEEE Trans. Commun.*, vol. 56, no. 7, pp. 1178–1188, Jul. 2008.

[46] Y. Tadokoro, K. Ito, J. Imai, N. Suzuki, and N. Itoh, "Advanced transmission cycle control scheme for autonomous decentralized TDMA protocol in safe driving support systems," in *2008 IEEE Intelligent Vehicles (IV) Symposium*, 2008, pp. 1062–1067.

[47] S. Mangold, C. Sunghyun, G. R. Hiertz, O. Klein, and B. Walke, "Analysis of IEEE 802.11e for QoS support in wireless LANs," *IEEE Wireless Commun.*, vol. 10, no. 6, pp. 40–50, Dec. 2003.

[48] X. Costa-Perez, D. Camps-Mur, and T. Sashihara, "Analysis of the integration of IEEE 802.11e capabilities in battery limited mobile devices," *IEEE Wireless Commun.*, vol. 12, no. 6, pp. 26–32, Dec. 2005.

[49] Network Simulator-3, https://www.nsnam.org/.

[50] J. M. Jornet and I. F. Akyildiz, "Channel modeling and capacity analysis for electromagnetic wireless nanonetworks in the terahertz band," *IEEE Trans. Wireless Commun.*, vol. 10, no. 10, pp. 3211–3221, Oct. 2011.

[51] K. Chi, Y. h. Zhu, X. Jiang, and V. C. M. Leung, "Energy-efficient prefix-Free codes for wireless nano-sensor networks using OOK modulation," *IEEE Trans. Wireless Commun.*, vol. 13, no. 5, pp. 2670–2682, May 2014.

[52] J. M. Jornet, J. C. Pujol, and J. S. Pareta, "PHLAME: a physical layer aware MAC protocol for electro-magnetic nanonetworks in the terahertz band," *Nano Commun. Networks*, vol. 3, no. 1, pp. 74–81, Mar. 2012.

[53] S. D'Oro, L. Galluccio, G. Morabito, and S. Palazzo, "A timing channel-based MAC protocol for energy-efficient nanonetworks," *Nano Commun. Networks*, vol. 6, no. 2, pp. 39–50, Jun. 2015.
[54] N. Rikhtegar, M. Keshtgari, and Z. Ronaghi, "EEWNSN: energy efficient wireless nano-sensor network MAC protocol for communications in the terahertz band," *Wireless Pers. Commun.*, vol. 97, no. 1, pp. 521–537, Nov. 2017.
[55] S. Hans and A. Nayyar, "A Review of De-Facto MAC Standard: IEEE 802.11 DCF," in *2014 Fourth Int. Conf. Adv. Comput. & Commun. Technol.*, 2014, pp. 372–376.
[56] C. Thorpe and L. Murphy, "A Survey of Adaptive Carrier Sensing Mechanisms for IEEE 802.11 Wireless Networks," *IEEE Commun. Surveys Tuts.*, vol. 16, no. 3, pp. 1266–1293, 3rd Quart. 2014.
[57] G. Bianchi, "Performance analysis of the IEEE 802.11 distributed coordination function," *IEEE J. Sel. Areas Commun.*, vol. 18, no. 3, pp. 535–547, Mar. 2000.
[58] N. Akkari P. Wang, J. M. Jornet, E. Fadel, L. Elrefaei, M. G. A. Malik, S. Almasri, and I. F. Akyildiz, "Distributed Timely Throughput Optimal Scheduling for the Internet of Nano-Things," *IEEE Internet Things J.*, vol. 3, no. 6, pp. 1202–1212, May 2016.
[59] S. Mohrehkesh and M. C. Weigle, "RIH-MAC: Receiver-Initiated Harvesting-aware MAC for NanoNetworks," *Proc. ACM The First Annual International Conference on Nanoscale Computing and Communication*, 2014.
[60] S. Mohrehkesh, M. C. Weigle, and S. K. Das, "DRIH-MAC: A Distributed Receiver-Initiated Harvesting-Aware MAC for Nanonetworks," *IEEE Trans. Mol. Biol. Multi-Scale Commun.*, vol. 1, no. 1, pp. 97–110, Aug. 2015.
[61] W. R. Heinzelman, A. Chandrakasan, and H. Balakrishnan, "Energy-efficient communication protocol for wireless microsensor networks," in *Proc. 33rd Annual Hawaii Int. Conf. System Sciences*, Jan. 2000.

Shoma Nishibori received the B.E. degree from the School of Engineering, Nagoya University in 2019, and Master of Informatics degree from the Graduate School of Informatics, Nagoya University, in 2021. He has been been involved in projects related to wireless sensor network, priority control of wireless communication. He received the Excellent Graduation Research Presentation Award on his research about MAC protocol for massive nanoscale sensor node in the Tokai Branch of IEICE in 2019.

Tutomu Murase (Member, IEEE) was born in Kyoto, Japan, in 1961. He received the M.E. degree from the Graduate School of Engineering Science, Osaka University, Japan, in 1986, and the Ph.D. degree from the Graduate School of Information Science and Technology, Osaka University, in 2004. He joined NEC Corporation Japan, in 1986. He was a Visiting Professor with the Tokyo Institute of Technology, from 2012 to 2014. He is currently a Professor with Nagoya University, Japan. He has been engaged in research on traffic management for high-quality and high-speed internet. His current interests include transport and session layer traffic control, wireless network resource management, and network security. He is also interested in user cooperative mobility research. Dr. Murase received the Best Tutorial Paper Award on his invited paper about QoS control for overlay networks in the IEICE Transactions on Communication in 2006. He has served as TPC for many IEEE conferences and workshops. He has more than 90 registered patents including several international patents. He was a Secretary of the IEEE Communications Society Japan Chapter. He is a Fellow of IEICE.

Yukihiro Tadokoro (M'00)–(SM'18) received the B.E., M.E., and Ph.D. degrees in information electronics engineering from Nagoya University, Aichi, Japan, in 2000, 2002, and 2005, respectively. Since 2006, he has been with Toyota Central R&D Labs., Inc., Japan. He was a Research Scholar with the Department of Physics and Astronomy, Michigan State University, East Lansing, MI, USA, in 2011 and 2012, to study nonlinear phenomena for future applications in signal and information processing fields. In 2019 and 2020, he was a Visiting Professor with the Graduate School of Informatics, Nagoya University. Since 2021, he has been an Executive Engineer in Toyota Research Institute of North America, Ann Arbor, MI, USA. His current research interests include nanoscale wireless communication, quantum sensing system, noise-related phenomena in nonlinear systems, and their applications in vehicles and smart cities. Dr. Tadokoro received two Best Paper Awards on his papers about stochastic resonance and noise-enhanced systems, in the IEICE Transactions on Communication and JSAP Applied Physics Express in 2021. Dr. Tadokoro is also a Senior Member of the Institute of Electronic, Information and Communication Engineers (IEICE) in Japan.